International Journal of Dental Research and Allied Sciences
2023, Volume 3, Issue 2, Page No: 24-28

Available online at: www.tsdp.net

ISSN: 3062-3502

Original Article

Innovative Approaches to Bone Density Assessment Using Volumetric Visualization

Mario A. de Oliveira[1*], Raimes Moraes[2], Everton B. Castanha[3], Alexandra S. Prevedello[4], Jozue Vieira Filho[5], Frederico A. Bussolaro[4], David García Cava[6]

[1]School of Engineering and the Built Environment, Birmingham City University, Birmingham, B47XG, United Kingdom.
[2]Department of Electrical and Electronic Engineering, Federal University of Santa Catarina, Florianopolis, 88040-900, Brazil.
[3]Faculty of Medicine, Federal University of Pelotas, Pelotas, 96030-000, Brazil.
[4]Health Science Institute, Federal University of Mato Grosso, Sinop, 78550-728, Brazil.
[5]Telecommunications and Aeronautical Engineering, São Paulo State University (UNESP), So Jlao da BoaVista, 13876-750, Brazil.
[6]School of Engineering, The Institute for Infrastructure and Environment, The University of Edinburgh, Edinburgh, EH93FG, United Kingdom.

***E-mail** ✉ mario.deoliveira@bcu.ac.uk

Received: 02 August 2023; **Revised:** 28 October 2023; **Accepted:** 30 October 2023

ABSTRACT

This study aimed to refine the method for spatial digital analysis of bone density. The experiment included spiral computed tomography (CT) scans of the facial skeleton of 20 patients aged 10 to 22 years with maxillofacial pathologies. The CT imaging was performed with slices aligned parallel to either the Frankfurt horizontal plane or the occlusal plane. The proposed method enables visualization and segmentation of bone tissue based on density levels within each scan, allowing for the precise identification of areas with the lowest and highest bone density. By isolating specific bone layers with defined density ranges, the technique facilitates their reconstruction and boundary tracing within a 3D volumetric model. This approach holds significant potential for applications in implantology, maxillofacial surgery, orthodontics, and periodontics aiding in the assessment of jawbone conditions and the planning of appropriate therapeutic interventions.

Keywords: X-ray density, Bones, 3D visualization, Computed tomography

How to Cite This Article: de Oliveira MA, Moraes R, Castanha EB, Prevedello AS, Filho JV, Bussolaro FA, et al. Innovative Approaches to Bone Density Assessment Using Volumetric Visualization. Int J Dent Res Allied Sci. 2023;3(2):24-8. https://doi.org/10.51847/FwflG3gghL

Introduction

When formulating treatment plans for orthodontic and surgical interventions in bone pathologies of the dental system, several factors are considered, including patient age, underlying systemic conditions, the condition of the bone tissue in the affected region, and the location of the pathological process. The latter plays a critical role in determining the type and extent of surgical procedures required [1-4].

Current X-ray imaging techniques allow for the assessment of the facial skeleton using both two-dimensional projections (radiography) and three-dimensional imaging (spiral computed tomography) [5, 6]. Spiral CT provides high-resolution images of bone structures in frontal, axial, and sagittal planes, along with volumetric SSD computer reconstructions. This enables precise identification of the location and extent of pathological changes in bone tissue while also allowing differentiation based on density [7-9].

Modern software tools support color mapping of bone tissue on axial sections according to density gradients, but this analysis remains confined to the axial plane. This limitation prevents a comprehensive stereoscopic spatial visualization of bone structure and, in some cases, may lead to misinterpretation of density zones due to variations in the scanning plane's inclination [10, 11]. While standardizing axial plane positioning during scanning can mitigate this issue, achieving an accurate three-dimensional representation of bone density distribution necessitates the development of enhanced analytical techniques [10-12].

The objective of this study was to refine and optimize the methodology for spatial digital analysis of bone density.

Materials and Methods

This study involved the analysis of archived spiral computed tomography (CT) data from 20 patients between the ages of 10 and 22 who presented with maxillofacial pathology. Spiral CT imaging of the facial skeleton was conducted to aid in diagnosis and treatment planning. The imaging procedure was standardized by ensuring that the CT scan slices were aligned either parallel to the Frankfurt horizontal plane or the occlusal plane **(Figure 1)**.

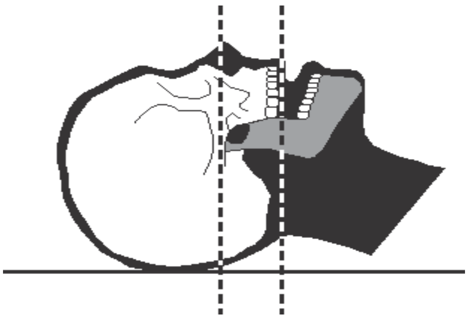

Figure 1. The layout of the axial slice plane during scanning

The computed tomography protocol for identifying bone tissue was developed based on previous research [13]. The Gantry tilt angle was set at 0°, and the reconstruction algorithm was configured for “bone” or “high-resolution” imaging. The matrix resolution was 512 × 512, with a slice thickness of 1 mm, a rotation step of 1 mm, and a reconstruction step of 1 mm. All archived data were saved in DICOM format and analyzed using the MATLAB R2006a software package and DICOM Works 1.3.5. Over 300 CT slices were examined and processed using specialized software, which involved isolating bone tissue by darkening soft tissues and applying specific markings **(Figure 2)**.

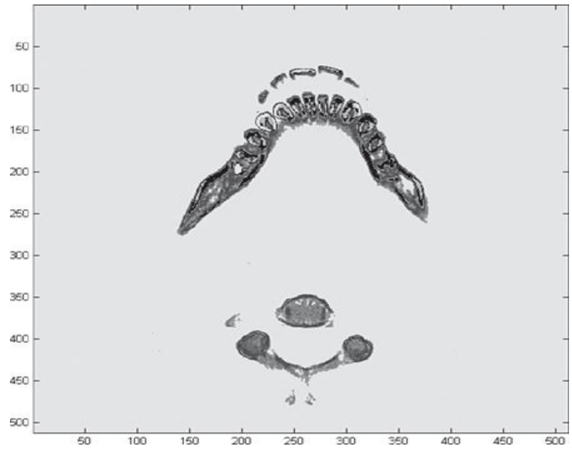

Figure 2. Image of axial section of jaw bone tissue.

Each bone density range was represented by a distinct color. The highest-density bone tissue, including teeth, was designated in black, whereas the lowest-density areas appeared in yellow. Intermediate densities were color-coded progressively from color green to blue, following the classification system outlined in the guidelines for the diagnostic management of incidental solitary bone lesions on CT and MRI [14].

To visualize the spatial distribution of bone density zones, a mathematical algorithm was developed using the MATLAB software platform. This algorithm, based on image matrix darkening with defined upper and lower thresholds, enabled the selective isolation of bone tissue within specific density ranges. This approach allowed for independent computer reconstruction of each density category. The resulting model was a solid-state 3D reconstruction with ring-marked zones representing four distinct levels of bone density.

Further analysis was conducted using DICOM Works 1.3.5, where the densitometric evaluation of the axial slice series was performed. This process assigned Hounsfield Unit (HU) values to the corresponding color spectra, ensuring precise density differentiation.

Results and Discussion

To establish the correlation between bone density and specific color indicators, the axial section of bone tissue was analyzed using the HSV color spectrum. In the initial series of axial slices, regions with the lowest bone density, falling within the range of 400-162 HU, were identified and represented in yellow and its varying shades **(Figure 3a)**.

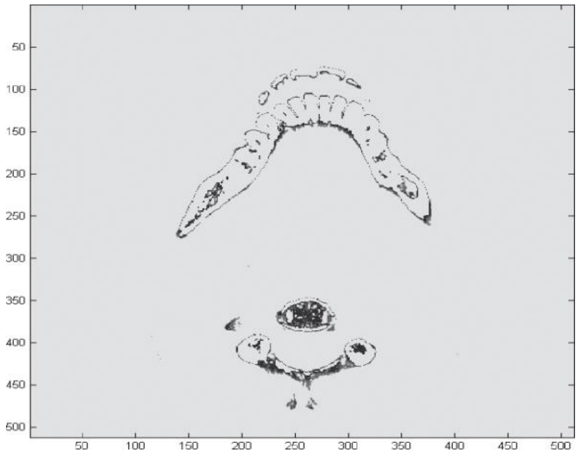

a)

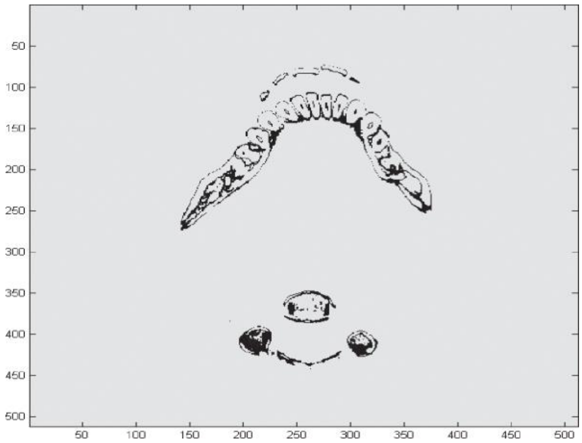

b)

Figure 3. Axial sections encoded in HSV color format: with a bone density range of 400-162 HU (a), with a bone density range of 678-469 HU (b).

In the second set of axial slices, applying matrix dimming within the range of 50 to 100 units in HSV mode allowed for the identification of bone tissue with a density between 678 and 469 HU. This region was distinctly visualized in varying shades of green **(Figure 3b)**.

For the third series of axial sections, adjusting the matrix dimming parameters to a lower threshold of 100 units and an upper limit of 190 units in HSV mode resulted in the segmentation of bone tissue with densities spanning from 1176 to 775 HU. These regions were rendered in blue and their gradient variations **(Figure 4a)**.

In contrast, the final set of axial slices posed a challenge when using the HSV color format, as the red-marked bone tissue blended with the background, complicating visual analysis and making quantitative computations unreliable **(Figure 4b)**. To overcome this issue, the RGB (jet) color format was implemented. By defining matrix dimming limits between 190 and 280 units in RGB mode and applying median and adaptive filtering, bone structures were successfully differentiated and displayed in red with their tonal variations **(Figure 5)**.

To construct a three-dimensional, color-coded visualization of bone tissue, SSD reconstruction was performed for each color component, corresponding to specific density values **(Figure 6a)**. The integration of these reconstructions produced a volumetric model of the facial skeleton, where the highest-density bone tissue (2107-1369 HU) appeared in red, while lower-density areas (400-162 HU) were represented in yellow **(Figure 6b)**.

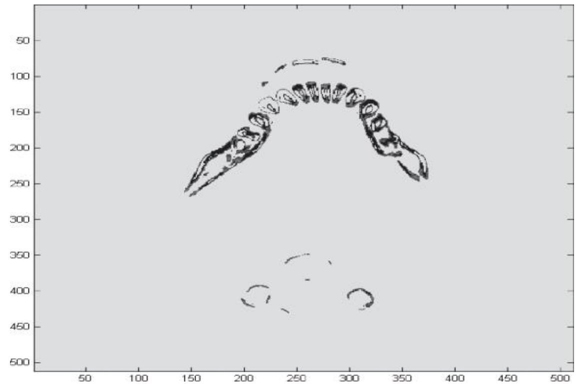

a)

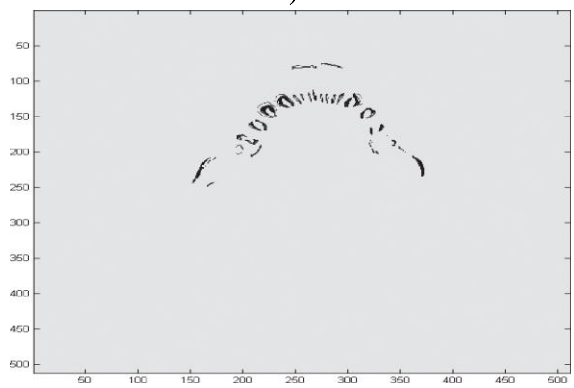

b)

Figure 4. Axial sections encoded in HSV format: with a bone density range of 1176-775 HU a), with a bone density range of 2107-1369 HU b)

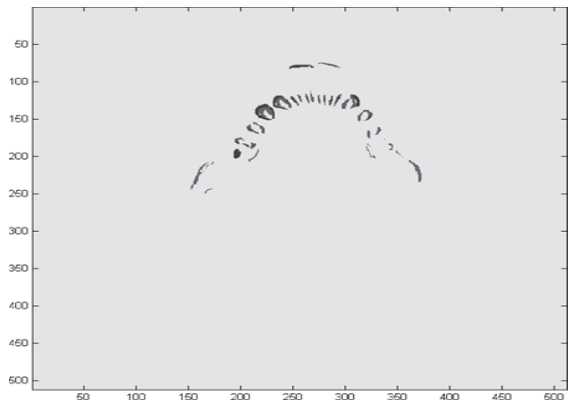

Figure 5. Axial slice encoded in RGB (jet) format with a bone density range of 2107-1369 HU

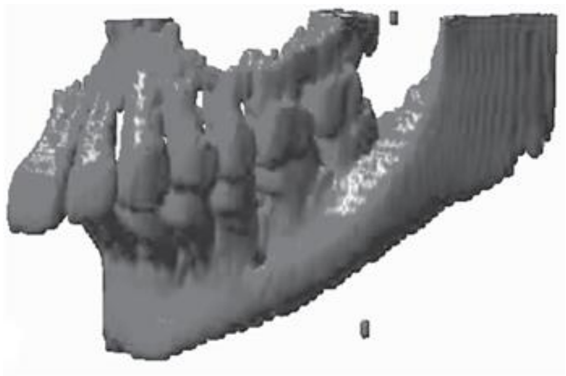

a)

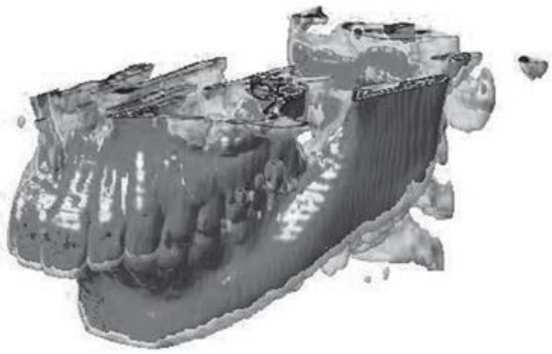

b)

Figure 6. Computer SSD reconstruction of the jaw bone: with a density range of 2107-1369 HU a); with a bone density range of 2107-1369 and 400-162 HU b)

Upon examining the generated image, it is evident that the bone density within the skull exhibits significant variation. Specifically, bone tissue with a density range of 2107-1369 HU is predominantly found in the frontal region of the upper jaw's alveolar process. The zygomatic-alveolar ridge contributes to the cortical layer in the angle, chin of the lower jaw, and the body. This area is also responsible for the marking of cement and dentin in the teeth [14]. These zones are distinctly visualized, with their borders easily identifiable in the resulting 3D reconstruction of the facial bones [15].

The analysis of computed tomography (CT) data further supports the consistency between the densitometric measurements and the images of the axial slices when decomposed into color spectra [16-19]. In other words, each color is directly associated with a specific bone density range, as demonstrated by the correlation between digital density values and their corresponding color spectra.

Conclusion

The method outlined in this study enables the visualization and categorization of bone tissue based on density, assigning each region to a specific color spectrum. This approach enhances the ability to identify areas of both high and low bone density. The ability to isolate and reconstruct individual bone layers according to their density range facilitates precise boundary tracing in a 3D computer model. This technique holds significant potential for application in fields such as periodontology, maxillofacial surgery, orthodontics, and implantology, providing valuable insights into the condition of the jawbone and aiding in the planning of targeted treatments.

Acknowledgments: None

Conflict of Interest: None

Financial Support: None

Ethics Statement: None

References

1. Roski F, Hammel J, Mei K, Baum T, Kirschke JS, Laugerette A, et al. Bone mineral density measurements derived from dual-layer spectral CT enable opportunistic screening for osteoporosis. Eur Radiol. 2019;29(11):6355-63. doi:10.1007/s00330-019-06263-z
2. Jin Z, Zhang F, Wang Y, Tian A, Zhang J, Chen M, et al. Single-photon emission computed tomography/computed tomography image-based radiomics for discriminating vertebral bone metastases from benign bone lesions in patients with tumors. Front Med. 2022;8:792581. doi:10.3389/fmed.2021.792581
3. Shevchenko YS, Plohova DP, Bulakhova IN, Mishvelov AE, Kubalova ME, Badriev GB, et al. Experience of carrying out magnetic resonance imaging with the use of specialized protocols and programs computer post-processing. Pharmacophore. 2020;11(2):77-81.
4. Mezhidov BS, Belyaeva AA, Kh SM, Bimarzaev S, Bektashev A, Shekhshebekova AM, et al. Prospects for creating 3D models of internal organs based on computer and magnetic resonance imaging images in emergency surgery and resuscitation. Pharmacophore. 2021;11(1):8-14. doi:10.51847/3TLcii4n42
5. Anderson AS, Sutherland ML, O'Donnell L, Hill EC, Hunt DR, Blackwell AD, et al. Do computed tomography findings agree with traditional osteological examination? The case of porous cranial lesions. Int J Paleopathol. 2021;33:209-19. doi:10.1016/j.ijpp.2021.04.008

6. Magomedova AS, Sheripovna DK, Kunkueva SA, Muskhanov MI, Ibragimov AK, Khazamova SO, et al. Application of a simulation system using augmented reality to practice the skills of minimally invasive spine surgery. J Pharm Res Int. 2021;33(42A):66-73. doi:10.9734/jpri/2021/v33i42A32385
7. Mishvelov AE, Ibragimov AK, Amaliev IT, Esuev AA, Remizov OV, Dzyuba MA, et al. Computer-assisted surgery: virtual-and augmented-reality displays for navigation during planning and performing surgery on large joints. Pharmacophore. 2021;12(2):32-8. doi:10.51847/50jmUfdufI
8. Suleymanov TA, Kosinkova AM, Mishvelov AE, Povetkin SN, Simonov AN, Ziruk IV. Overview of the holodoctor software package. Pharmacophore. 2020;11(2):65-72.
9. Tovlahanova TJ, Suleimanova MU, Dzaurova LH, Mezhieva MM, Murtazalieva BM, Durniyazov MN, et al. Study of the effect of the image scanning speed and the type of conductive coating on the quality of sem-micrographs of oxide Nano materials for medical use. Ann Med Health Sci Res. 2021;11(S3):60-4.
10. Valiukhov DP, Baklanov IS, Shtab EV, Shtab AV, Pigulev RV, Iliasov AS. Resonant-frequency properties of low-dimensional junction of semiconductor-metal-semiconductor and calculation methodology. InJournal of physics: conference series 2019 (Vol. 1384, No. 1, p. 012002). IOP Publishing.
11. Maisigov JB, Kuznetsova GV, Magomedov AM, Adzhigova FZ, Magomedova AS, Burdukova SA, et al. Anthropometric analysis of digital models of the dentition using 3D technologies in orthodontics. J Pharm Res Int. 2021;33(39B):101-5.
12. van Oosterom MN, van der Poel HG, Navab N, van de Velde CJH, van Leeuwen FWB. Computer-assisted surgery: virtual- and augmented-reality displays for navigation during urological interventions. Curr Opin Urol. 2018;28(2):205-13. doi:10.1097/MOU.0000000000000478
13. Nagdalian AA, Rzhepakovsky IV, Siddiqui SA, Piskov SI, Oboturova NP, Timchenko LD. Analysis of the content of mechanically separated poultry meat in sausage using computing microtomography. J Food Compost Anal. 2021;100(4):103918. doi:10.1016/j.jfca.2021.103918
14. Chang CY, Garner HW, Ahlawat S, Amini B, Bucknor MD, Flug JA, et al. Society of skeletal radiology–white paper. Guidelines for the diagnostic management of incidental solitary bone lesions on CT and MRI in adults: bone reporting and data system (Bone-RADS). Skeletal Radiol. 2022;51(9):1743-64. doi:10.1007/s00256-022-04022-8
15. Galabueva AI, Biragova AK, Kotsoyeva GA, Borukayeva ZK, Yesiev RK, Dzgoeva ZG, et al. Optimization of modern methods of treating chronic generalized periodontitis of mild severity. Pharmacophore. 2020;11(1):47-51.
16. Asgari I, Soltani S, Sadeghi SM. Effects of iron products on decay, tooth microhardness, and dental discoloration: a systematic review. Arch Pharm Pract. 2020;11(1):60-82.
17. Alamri AM, Alshammery HM, Almughamis MA, Alissa AS, Almadhi WH, Alsharif AM, et al. Dental recession aetiology, classification and management. Arch Pharm Pract. 2019;10(2):28-31.
18. Remizova AA, Dzgoeva MG, Tingaeva YI, Hubulov SA, Gutnov VM, Bitarov PA. Tissue dental status and features of periodontal microcirculation in patients with new COVID-19 coronavirus infection. Pharmacophore. 2021;12(2):6-13. doi:10.51847/5JIbnUbHkT
19. Holland P, Quintana EM, Khezri R, Schoborg TA, Rusten TE. Computed tomography with segmentation and quantification of individual organs in a D. melanogaster tumor model. Sci Rep. 2022;12(1):2056. doi:10.1038/s41598-022-05991-5